



## Dynamic constitutive relationship of TiZrHfCu0.5 high entropy alloy based on Johnson-Cook model

Chuang Chen<sup>\*</sup>, Yiliang Tu, Junlin Chen, Enling Tang

Key Laboratory of Transient Physical Mechanics and Energy Conversion Materials of Liaoning Province, Shenyang Ligong University, Shenyang 110159, China

### ARTICLE INFO

**Keywords:**

High entropy alloy  
Mechanical properties  
Constitutive model  
Low temperature

### ABSTRACT

High entropy alloy has attracted much attention in the field of national defense due to their excellent low-temperature dynamic mechanical properties. Taking TiZrHfCu0.5 high entropy alloy as the research object, the compressive properties of the specimens under quasi-static and dynamic (strain rate range  $600\text{s}^{-1}$ - $2600\text{s}^{-1}$  and temperature range  $-60\text{ }^{\circ}\text{C}$ - $20\text{ }^{\circ}\text{C}$ ) conditions are systematically tested. Based on the static/dynamic stress-strain experimental results, the parameters of the original Johnson-Cook constitutive model are determined by fitting. On this basis, a modified Johnson-Cook constitutive model considering the coupling effects of strain, strain rate and temperature is proposed and its parameters are determined. The dynamic compression process of the specimens under different strain rates and temperatures is numerically simulated by ABAQUS finite element software, and the accuracy of the modified Johnson-Cook constitutive model to predict the dynamic compression behavior of TiZrHfCu0.5 high entropy alloy is verified. The experimental and numerical simulation results show that the TiZrHfCu0.5 high entropy alloy exhibits significant strain rate hardening effect and excellent low-temperature mechanical properties during dynamic compression. The ultimate stress can reach 1.79 GPa at  $-20\text{ }^{\circ}\text{C}$  and strain rate of  $2600\text{ s}^{-1}$ . The predicted curves of the modified Johnson-cook constitutive model are in good agreement with the experimental results at low temperature and high strain rate. The modified Johnson-Cook constitutive model is embedded in the finite element software, which effectively improves the reliability of the numerical simulation of the compression performance of TiZrHfCu0.5 high entropy alloy at high strain rate and low temperature. The relative error between the predicted results of the modified Johnson-Cook constitutive model and the experimental results is greatly reduced.

### 1. Introduction

The major challenge faced by modern material science is to develop high-performance materials to meet the rapid development of science and technology. A large number of engineering application materials have been developed based on the traditional concept of test specimens with one or two elements as the main component to improve the performance. However, the ability of material composition and organization optimization is limited, and the performance improvement has reached the bottleneck, which cannot meet the urgent demand for higher-performance materials in various fields. In 2004, the design concept of high entropy alloy (HEA) was put forward. Its unique alloy design concept can reflect the clustering effect of various alloy elements. High entropy alloy has excellent properties such as high strength, high density, high hardness, good plasticity, wear resistance and corrosion resistance [1,2]. It is widely used in the field of national defense under

high strain rate. In particular, refractory high entropy alloy exhibits excellent mechanical properties in extreme environments such as high strain rates and low temperatures due to their unique microstructure [3,4]. As a highly promising structural and functional material, high entropy alloy has enormous application potential in extreme environments such as high strain rates and low temperatures. It is of great significance to investigate the mechanical response and dynamic constitutive model of high entropy alloy under coupling conditions of low temperature and high strain rate.

In recent years, scholars have carried out extensive research on the dynamic mechanical properties of HEA at a wide range of strain rates and temperatures. Hu M L [5] et al. investigated the mechanical behavior of TaNbHfZrTi refractory high-entropy alloy (RHEA) at strain rate up to  $2600\text{s}^{-1}$  and temperatures from 77K to 873K. The results showed that the yield strength was increased significantly at high strain rates and high temperatures. The fracture morphology investigated by

\* Corresponding author.

E-mail addresses: [chenchuang517@126.com](mailto:chenchuang517@126.com), [chenchuang@sylu.edu.cn](mailto:chenchuang@sylu.edu.cn) (C. Chen).



scanning electron microscopy indicated both ductile and brittle fracture behavior of the TaNbHfZrTi RHEA at 77K. Wang S B [6] et al. explored the tensile properties of TiZrHfNbTa high entropy alloy at cryogenic temperatures. The results showed that the alloy maintained a high tensile elongation of 20.8 % while the yield strength increased significantly up to 1549 MPa as the temperature was decreased from 277 K to 77 K, without obvious ductile to brittle transition. Chen J L [7] et al. investigated the dynamic mechanical properties of TiZrHfX<sub>0.5</sub> high-entropy alloys associated with temperature, trace element and strain rate. The ultimate strength of TiZrHfCu<sub>0.5</sub> and TiZrHfNi<sub>0.5</sub> specimens were significantly increased with the decreasing of temperature. Ren K R [8] et al. explored the dynamic compression behavior of TiZrNbV refractory high-entropy alloys upon ultrahigh strain rate loading. Microstructural analysis showed that the dynamic deformation of the TiZrNbV RHEA was controlled by the dislocation slip, dislocation proliferation, intersection of the deformation bands, and grain refinement. Sun J [9] et al. investigated the effect of temperature and strain rate on quasi-static and dynamic compressive behavior of forged CrMnFeCoNi high entropy alloy. The results showed that the strain hardening rate increased with the decrease of temperature under both quasi-static and dynamic conditions, while strain rate sensitivity was exhibited only at high temperatures. Zhong X Z [10] et al. investigated the dynamic compressive properties and microstructural evolution of Al<sub>1.19</sub>Cu<sub>2</sub>CrFeNi<sub>1.81</sub> eutectic high entropy alloy at room and cryogenic temperatures. The results showed that the eutectic high entropy alloy exhibited an excellent strength-plasticity combination, especially at the strain rate of 4300 s<sup>-1</sup> at 77 K, showing a yield strength of 1365 MPa and a true plastic strain over 40 %. The fractographic observations showed a transition from ductile to mixed ductile-brittle fracture mode with decreasing temperature.

Moreover, the construction of high entropy alloy constitutive model is the key to evaluate the performance of materials under strong dynamic load by finite element numerical simulation. Yuan K B [11] et al. developed a viscoplastic constitutive model considering the microstructural features, which could reflect the size effect of grains and phases on flow stress, as well as the influence of the phase content on the rate-temperature coupling effect. This model was demonstrated to successfully predict the dynamic plastic flow behavior of eutectic high entropy alloy over a wide range of temperature. Zhao D [12] et al. proposed a constitutive model based on the crystal plasticity theory, and the constitutive model validation was performed by comparing numerical results with experimental data. Wang Y Y [13] et al. developed a crystal plasticity constitutive model of high-entropy alloys coupled with damage evolution equation at high temperature. The constitutive model was used to simulate the stress softening phenomenon of polycrystalline AlCrCuFeNi-based high-entropy alloys, which was highly dependent on the strain rate and temperature. Brown C [14] et al. developed plastic flow stress models for a variety of existing constitutive models, namely, the Johnson-Cook, modified Johnson-Cook, Zerilli-Armstrong, modified Zerilli-Armstrong, Zener-Hollomon, Hensel-Spittel, and modified Hensel-Spittel. The results showed that the modified Johnson-Cook, Zener-Hollomon, Hensel-Spittel, and modified Hensel-Spittel models were all found to provide reasonable predictive accuracy for CoCr-FeMnNi. Zhang T W [15] et al. established the modified Johnson-Cook model considering the adiabatic temperature rise converted by plastic deformation work at high strain rates, which was used to characterize the flow behavior of AlCoCr<sub>1.5</sub>Fe<sub>1.5</sub>NiTi<sub>0.5</sub> high-entropy alloy. Kim Y [16] et al. investigated the constitutive modeling of CoCrFeMnNi high-entropy alloy at cryogenic temperature (77 K) and room temperature (293 K). The effects of temperature on twinning and dislocation slip were quantitatively analyzed by ABAQUS finite element software. Wang Y Z [17] et al. investigated the dynamic tension properties of Fe<sub>40</sub>Mn<sub>20</sub>Cr<sub>20</sub>Ni<sub>20</sub> high-entropy alloys with a heterogeneous structure, and employed a typical Johnson-Cook model to predict the dynamic-flow behavior. Sun Z R [18] et al. investigated the mechanical behavior and constitutive modeling for as-cast Al<sub>0.3</sub>CoCrFeNi high

entropy alloy. The constitutive behavior of the alloy was characterized using the modified Johnson-Cook model. The modified Johnson-Cook model demonstrated predictions within a 10 % deviation from experimental data. Jain R [19] et al. predicted the hot deformation behavior of CoFeMnNiTi eutectic high-entropy alloy by using the Arrhenius-type constitutive equation and artificial neural network (ANN) model in the temperature range 1073–1273 K and strain rate range 0.001–1 s<sup>-1</sup>. The performance of both models was assessed by using the coefficient of correlation and average absolute relative error. In summary, the Johnson-Cook constitutive model can effectively predict the dynamic mechanical properties of high entropy alloy. However, the original Johnson-Cook constitutive model assumes that strain hardening, strain rate strengthening, and temperature effects are independent of each other. In fact, the coupling effect of strain, strain rate, and temperature cannot be ignored. Therefore, it is necessary to modify the Johnson-Cook constitutive model to achieve reliable and efficient prediction of the dynamic mechanical properties of high entropy alloy.

In this study, TiZrHfCu0.5 high entropy alloy ingots are prepared by vacuum arc melting process. The compression properties of TiZrHfCu0.5 high entropy alloy at different strain rates and temperatures are carried out by universal testing machine and SHPB experimental system. A modified Johnson-Cook constitutive model considering the coupling effects of strain, strain rate and temperature is developed to predict the low-temperature dynamic mechanical behavior of TiZrHfCu0.5 high entropy alloy. The parameters of the original Johnson-Cook and the modified Johnson-Cook constitutive model are determined by fitting the stress-strain experimental data, and the modified Johnson-Cook constitutive model is introduced into the ABAQUS finite element software. The reliability of the modified Johnson-Cook constitutive model is verified by comparing the experimental and simulation data.

## 2. Materials and methods

TiZrHfCu0.5 high entropy alloy was prepared by vacuum arc melting process. Quasi-static and dynamic compression experiments at different temperatures and strain rates were carried out, respectively. Based on the obtained true stress-strain curves, the parameters of the original Johnson-Cook constitutive model and the modified Johnson-Cook constitutive model were determined by fitting. The modified Johnson-Cook constitutive model was applied to ABAQUS finite element software to carry out SHPB numerical simulation under corresponding experimental conditions. The accuracy of the modified Johnson-Cook constitutive model was verified by calculating the relative error. Fig. 1 is the flow chart of research content.

### 2.1. Specimen preparation

TiZrHfCu0.5 high entropy alloy ingots were prepared by vacuum arc melting process. 0.5 at % Cu particles were added to the mixed cylindrical particles of Ti, Zr and Hf with equal atomic ratio. According to the melting point from high to low, the particles were placed in the water-cooled crucible of the electric arc furnace, and the melting furnace was vacuumed. The high purity argon with a purity of 99.99 % was introduced to the furnace pressure of 0.05 MPa. In the process of vacuum arc melting, in order to make the elements mixed evenly, the alloy ingot was turned and melted 9 times for 5 min each time, and the electromagnetic stirrer was turned on for stirring. After the melting was completed, it was cooled to room temperature for sampling to obtain a high entropy alloy ingot. Finally, the corresponding size of the specimen was obtained by wire cutting. The specimens were polished with 800 #, 1200 # and 1500 # sandpaper to remove surface impurities, respectively.

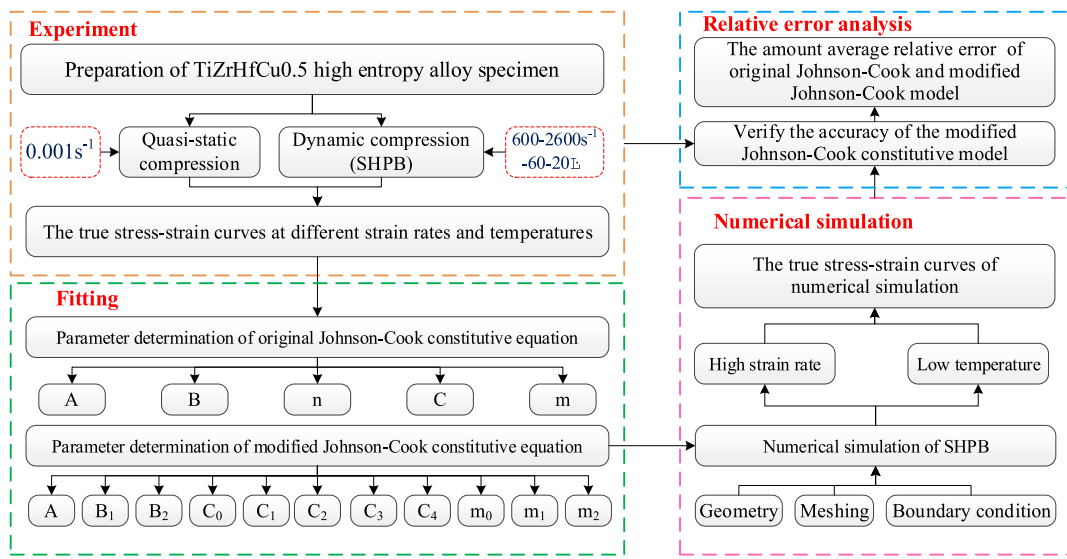


Fig. 1. The flow chart of research content.

## 2.2. Experiment

### 2.2.1. Quasi-static compression experiment

The quasi-static compression experiment was carried out by electronic universal testing machine at room temperature (20 °C). The specimen was placed on the steel anvil to keep it in the center position. The initial strain rate was 0.001 s<sup>-1</sup> during the test, and the specimen size was Φ6mm × 3.6 mm. In the quasi-static compression test, the engineering stress-strain curve of the specimen was recorded by the computer acquisition system equipped with the universal testing machine. The true stress and strain are calculated by formula (1) and (2).

$$\sigma_T = (1 - \varepsilon)\sigma \quad (1)$$

$$\varepsilon_T = -\ln(1 - \varepsilon) \quad (2)$$

Where  $\sigma_T$  and  $\varepsilon_T$  represent true stress and strain, respectively;  $\sigma$  and  $\varepsilon$  are the engineering stress and strain, respectively.

### 2.2.2. SHPB experiment

Separate Hopkinson pressure bar (SHPB) is widely used to measure the dynamic mechanical properties of materials [20]. The schematic diagram of the experimental system is shown in Fig. 2. The experimental device consists of an impact bar, an incident bar, a transmission bar, a buffer bar, a high-pressure gas source and a gas chamber. The diameters of the pressure bars are all 16 mm, the lengths of the incidence and transmission bars are both 1200 mm, and the length of the impact bar is 200 mm. When conducting low-temperature experiments, the temperature of the specimen is reduced by liquid nitrogen. The size of the specimen is Φ6mm × 3.6 mm. The ambient temperature is monitored by

thermocouple to ensure that the specimen reaches the experimental temperature (0 ~ –60 °C). A high-speed camera system is used to record the dynamic deformation process during shock compression.

The original signals of incident pulse  $\varepsilon_i(t)$ , transmitted pulse  $\varepsilon_t(t)$  and reflected pulse  $\varepsilon_r(t)$  are recorded by strain gauges. Fig. 3(a) shows the original waveforms during the dynamic compression process. The relationship among  $\varepsilon_i(t)$ ,  $\varepsilon_t(t)$  and  $\varepsilon_r(t)$  is

$$\varepsilon_i(t) = \varepsilon_t(t) + \varepsilon_r(t) \quad (3)$$

Based on the one-dimensional stress wave propagation theory, the stress, strain and strain rate of the specimen are solved by using Eqs (4)–(6) [21]. The experimental data are processed by the two-wave method to obtain the stress-strain relationship curve of the specimen. Fig. 3(b) shows the original waveforms and stress balance images obtained from the compression experiments.

$$\dot{\varepsilon}(t) = -\frac{2c}{l_s} \varepsilon_r(t) \quad (4)$$

$$\varepsilon(t) = -\frac{2c}{l_s} \int_0^t \varepsilon_r(t) dt \quad (5)$$

$$\sigma(t) = \frac{A}{A_s} E \varepsilon_t \quad (6)$$

Where  $c$ ,  $E$  and  $A$  are the elastic wave velocity, elastic modulus and cross-sectional area of the bar;  $l_s$  and  $A_s$  are the length and cross-sectional area of the specimen.

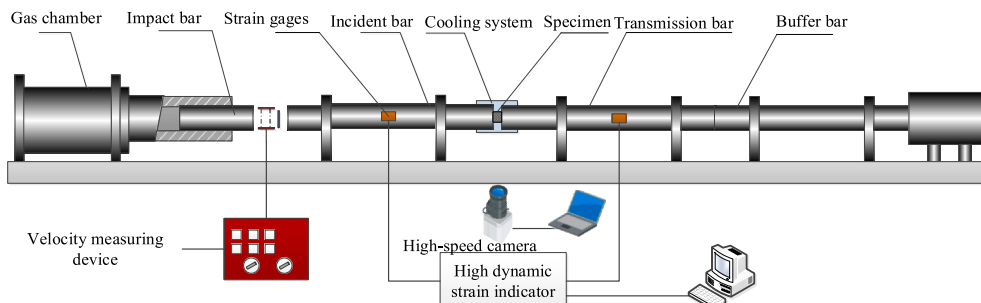


Fig. 2. The schematic diagram of the experimental system.

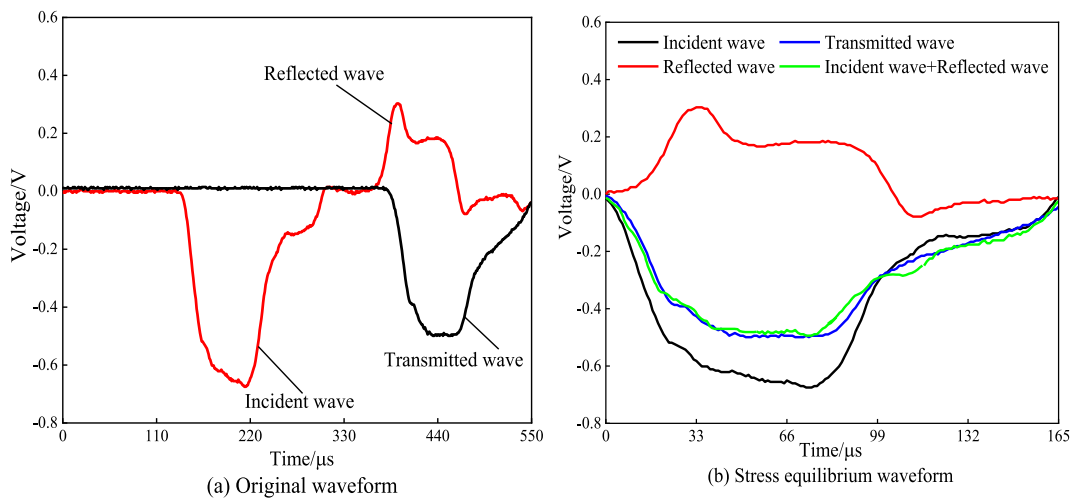


Fig. 3. Original waveform and stress balance waveform of SHPB.

### 2.2.3. Experimental parameters

In order to establish the dynamic constitutive equation of TiZrHfCu0.5 high entropy alloy and determine its parameters, static and dynamic compression experiments at different strain rates and different temperatures are carried out. Table 1 shows the loading conditions for quasi-static and dynamic compression at different strain rates. Table 2 shows the dynamic compression loading conditions at different temperatures.

### 2.3. Numerical simulation

#### 2.3.1. Finite element model

To verify the reliability of the modified Johnson-Cook constitutive model under different strain rates and temperatures, the finite element software ABAQUS/CAE is used for numerical simulation. The simulation model is established according to geometric characteristics of SHPB system as shown in Fig. 4.

Incident bar, impact bar, specimen and transmission bar are four parts of the simulation model. The structured hexahedral mesh is used for discretization, and then the numerical simulation geometric model corresponding to each experiment is established. The model size is in agreement with the SHPB experiment. The contacts between the bar and the bar, the bar and the specimen are defined as the surface-to-surface contact. In the numerical simulation, by adjusting the impact bar speed, the experimental conditions of different strain rates and temperatures loading are simulated. In the analysis step, the explicit dynamics is selected, and the displacement constraints of the specimen model and the bar are set in the x and y directions. At the same time, fixed constraints are set on the end face of the transmission rod in the z direction, and the initial conditions of the impact bar are set according to the velocity of the impact bar measured by the experiment. Fig. 5 is the simulation flow chart.

Table 1

The loading conditions for quasi-static and dynamic compression at different strain rates.

No.	Specimen	Temperature/°C	Loading speed/m·s <sup>-1</sup>
1	TiZrHfCu0.5	20	$3.6 \times 10^{-6}$
2			3.3
3			6.5
4			10.05
5			18.9
6			18.8
7			19.8

Table 2

The dynamic compression loading conditions at different temperatures.

No.	Specimen	Loading speed/m·s <sup>-1</sup>	Temperature/°C
8	TiZrHfCu0.5	19.8	20
9		18.09	0
10		17.73	-20
11		17.2	-40
12		17.53	-60

#### 2.3.2. Johnson-Cook model

The constitutive equations are commonly used to predict the dynamic behavior of materials and include basic physical constitutive models, phenomenological constitutive models, and neural network-based modeling. The phenomenological constitutive models can be determined by fitting experimental data and regression analysis. Therefore, the phenomenological constitutive model is more suitable than the basic physical constitutive model for predicting the dynamic behavior of materials at different strain rates and temperatures and is more easily referenced in finite element programs.

The Johnson-Cook constitutive model includes strain, strain-rate hardening effect and temperature softening effect. Due to its simple form, clear physical meaning and easy to obtain parameters, it has been widely and successfully applied to the impact of metal structures and nonlinear large deformation problems. It is also the most commonly used phenomenological constitutive model to predict the dynamic behavior of materials. The Johnson-Cook constitutive model [22] is as follows.

$$\sigma = (A + B\epsilon^n)(1 + C \ln \dot{\epsilon}^*)(1 - T^{*m}) \quad (7)$$

Where A and B are the yield strength and strain hardening coefficient of the material at the reference strain rate and reference temperature; n is the strain hardening index of the material at the reference strain rate and reference temperature; C is the strain rate sensitivity coefficient; m is the temperature softening index;  $\epsilon$  is the equivalent plastic strain;  $\dot{\epsilon}^*$  is the dimensionless equivalent plastic strain rate,  $\dot{\epsilon}^* = \dot{\epsilon}/\dot{\epsilon}_0$ ,  $\dot{\epsilon}_0$  is the reference strain rate;  $T^*$  is a dimensionless temperature parameter,  $T^* = (T - T_r)/(T_m - T_r)$ , T is the current temperature of the material,  $T_r$  is the reference temperature, generally selected as room temperature, and  $T_m$  is the melting point of the material.

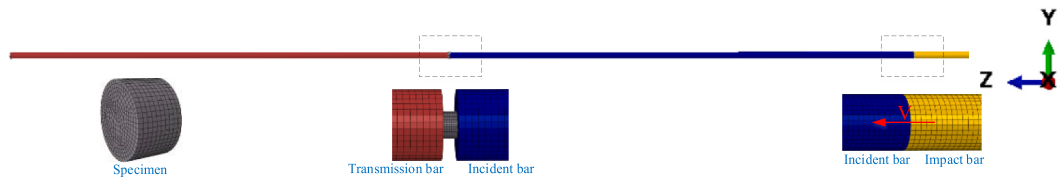


Fig. 4. SHPB finite element model.

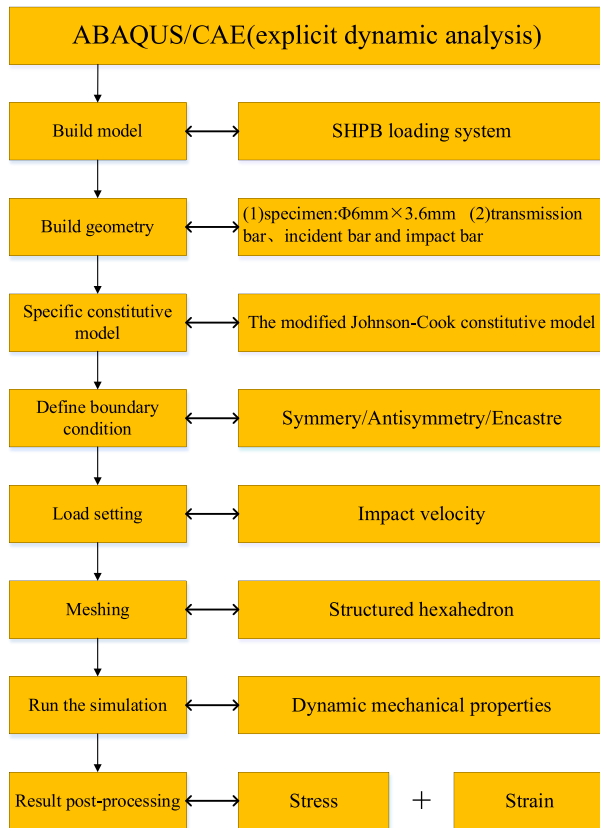


Fig. 5. The simulation flow chart.

### 3. Results and discussion

#### 3.1. Quasi-static mechanical properties

The true stress-strain curve of the quasi-static compression experiment is shown in Fig. 6. The yield stress is estimated according to the intersection of the elastic and the extension line of the plastic phase. As can be seen from the figure, with the increase of strain, the stress of the specimen also increases, and the maximum stress reaches 1.2 GPa. It is shown that TiZrHfCu0.5 has obvious strain hardening behavior during quasi-static compression. In the Johnson-Cook constitutive equation,  $\varepsilon$  is the equivalent plastic strain, and the effective stress-strain curve of the Johnson-Cook model can be obtained by subtracting the part before the yield strength of the true stress-strain curve.

#### 3.2. Strain rate hardening effect

The true stress-strain curves of TiZrHfCu0.5 HEA with different strain rates at room temperature are shown in Fig. 7(a). At the same strain, the true stress of the specimen increases with the increase of strain rate, which belongs to the strain rate hardening effect. According to the stress-strain curves, the yield stresses of TiZrHfCu0.5 at room

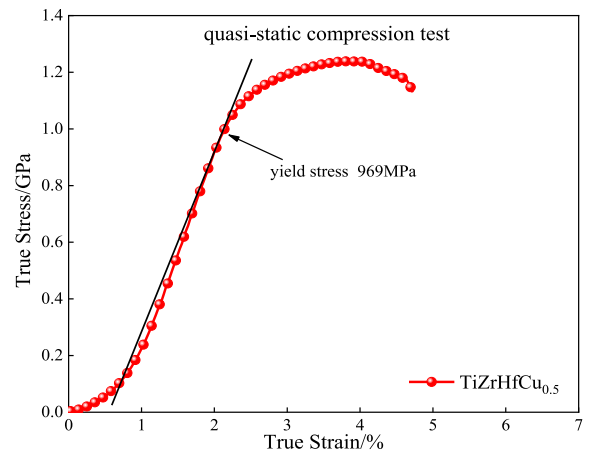


Fig. 6. The true stress-strain curve of quasi-static compression experiment.

temperature with different strain rates can be derived, as shown in Table 3. When the strain rate increases from  $600\text{s}^{-1}$  to  $2600\text{s}^{-1}$ , the yield stress increases from 0.92 GPa to 1.32 GPa. The results indicate that TiZrHfCu0.5 HEA has a significant strain rate hardening effect. Fig. 7(b) shows the repeatability experiment under the condition of high strain rate. It can be seen that the stress-strain curve of TiZrHfCu0.5 is basically consistent under the same loading rate.

#### 3.3. Low-temperature dynamic mechanical properties

Fig. 8 shows the true stress-strain curves at different temperatures. At the same strain rate ( $2600\text{s}^{-1}$ ), the true stresses of the specimens increase with the decrease of temperature except at  $-60^\circ\text{C}$ , indicating that TiZrHfCu0.5 exhibits excellent mechanical properties at low temperatures. When the temperature decreases, for the body-centered cubic metal, the true stress that has a strong dependence on temperature is mainly the Peierls-Nabarro stress, which belongs to the short-range resistance [23,24]. In low-temperature dynamic compression experiments, the specimens produce hardening phenomena and dislocation slip is hindered to increase the short-range resistance. The existence of chemical short-range order (CSRO) during impact will cause the fluctuation of dislocation energy in the alloy, which will lead to the fluctuation of dislocation slip lattice resistance, and then activate various deformation mechanisms such as dislocation pinning, cross slip and twinning, ultimately promoting the improvement of the system strength and toughness [25]. At  $-60^\circ\text{C}$ , a cold brittle transition may occur within the specimen due to the lower temperature, resulting in the decrease of plasticity and stress of the specimen.

Based on the experimental results, the ultimate stresses of TiZrHfCu0.5 HEA at different temperatures can be derived, as shown in Table 4. When the temperature is reduced from  $20^\circ\text{C}$  to  $-60^\circ\text{C}$ , the ultimate strength of the specimen increases from 1.56 GPa to 1.79 GPa.

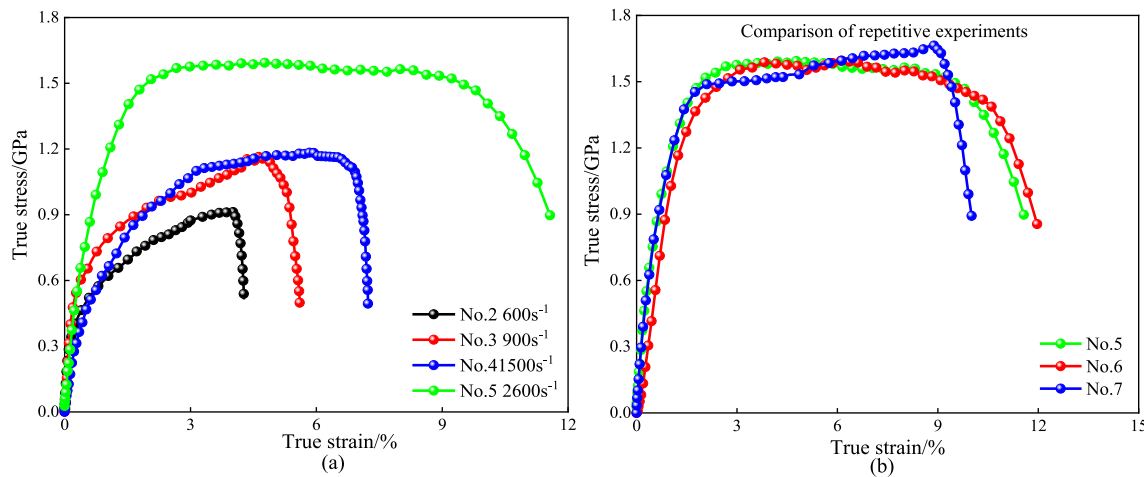


Fig. 7. The true stress-strain curves of TiZrHfCu0.5 HEA. (a) No. 2- No. 5 (b) No. 5- No. 7.

Table 3

Yield stress of TiZrHfCu0.5 with different strain rates at room temperature.

Strain rate/s <sup>-1</sup>	0.001	600	900	1500	2600
Yield stress/GPa	0.89	0.92	1.15	1.20	1.32

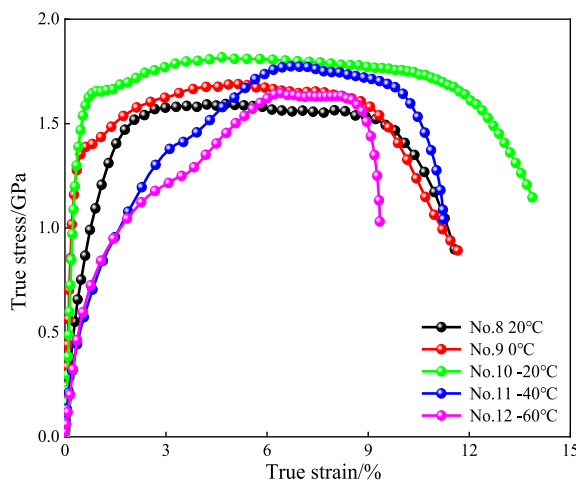


Fig. 8. The true stress-strain curves of TiZrHfCu0.5 at different temperatures.

Table 4

Ultimate strength of TiZrHfCu0.5 at different temperatures.

Temperature/°C	20	0	-20	-40	-60
Ultimate strength/GPa	1.56	1.64	1.79	1.77	1.64

#### 4. Parameter determination of Johnson-Cook constitutive equation

##### 4.1. Original Johnson-Cook model

In summary, all five parameters of the Johnson-Cook model are determined from experimental data. Taking into account the effects of three items in the constitutive equation corresponding to strain hardening, strain rate strengthening and temperature, the parameters can be determined one by one based on the above experimental results.

##### 4.1.1. Determination of parameters A, B and n

In the quasi-static compression state at room temperature, the reference strain rate is  $0.001 \text{ s}^{-1}$ . The strain rate hardening term and the temperature term in the Johnson-Cook model are both 1, and only the strain hardening term is retained.

$$\sigma = A + Be^n \quad (8)$$

From the quasi-static compression image (Fig. 6), the yield stress of TiZrHfCu0.5 can be obtained as 969 MPa, i.e.,  $A = 969 \text{ MPa}$ . Take the logarithm at both ends of formula (8) to obtain

$$\ln(\sigma - A) = \ln B + n \ln \epsilon \quad (9)$$

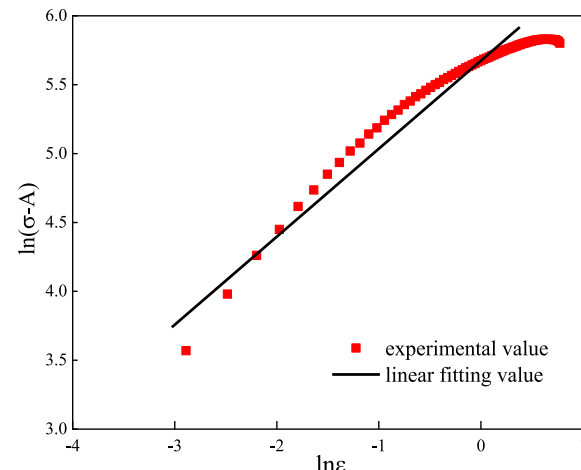
Substituting the value of A, the relationship between  $\ln(\sigma - A)$  and  $\ln \epsilon$  is obtained from the experimental data, as shown in Fig. 9. The values of constants B and n can be obtained from the intercept and slope of the fitted curve in the figure, i.e.,  $B = 1076 \text{ MPa}$  and  $n = 0.90$ .

##### 4.1.2. Determination of strain rate hardening coefficient C

In the room temperature SHPB experiment, the temperature term is 1 due to  $T^* = 0$ . From the deformation of formula (7), it can be obtained.

$$\frac{\sigma}{A + Be^n} = C \ln \dot{\epsilon}^* + 1 \quad (10)$$

The value of C can be obtained from the slope of the fitting curve in Fig. 10. Based on the experimental data, the strains of 0.02–0.06 are selected to determine the relationship between  $[\sigma/(A + B^n)]$  and  $\ln \dot{\epsilon}^*$ .

Fig. 9. The relationship between  $\ln(\sigma - A)$  and  $\ln \epsilon$

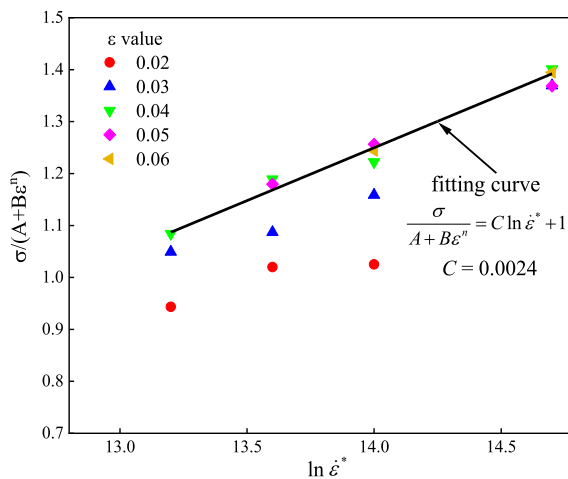


Fig. 10. The relationship between  $[\sigma / (A + B\dot{\varepsilon}^n)]$  and  $\ln \dot{\varepsilon}^*$ .

The data are fitted to obtain the fitting curve to calculate the C value, i.e.,  $C = 0.0024$ , as shown in Fig. 10.

#### 4.1.3. Determination of thermal softening coefficient m

In order to determine the constant  $m$  in Johnson-Cook model, the deformation formula (7) can be obtained.

$$\ln([\sigma / (A + B\dot{\varepsilon}^n)(1 + C \ln \dot{\varepsilon}^*)] - 1) = m \ln(-T^*) \quad (T^* < 0) \quad (11)$$

The true stresses corresponding to different temperatures and different strains are substituted into equation (11) to obtain the relationship between  $\ln(1 - \sigma / [(A + B\dot{\varepsilon}^n)(1 + C \ln \dot{\varepsilon}^*)])$  and  $\ln -T^*$ , as shown in Fig. 11. Finally,  $m = 0.503$  is obtained by linear fitting.

The original Johnson-Cook model parameters of the TiZrHfCu0.5 high entropy alloy are shown in Table 5.

From the above table, the original Johnson-Cook model can be expressed as

$$\sigma = (969 + 1076\varepsilon^{0.90})(1 + 0.0024\dot{\varepsilon}^*) \left[ 1 - (-T^*)^{0.503} \right] \quad (12)$$

#### 4.1.4. Parameter verification of original Johnson-cook constitutive model

To verify the accuracy of the original Johnson-Cook model, SHPB experimental results and original Johnson-Cook model predicted curves are compared at different strain rates and temperatures.

The stress-strain comparison between SHPB experimental results and original Johnson-Cook model predicted curves with different strain rates

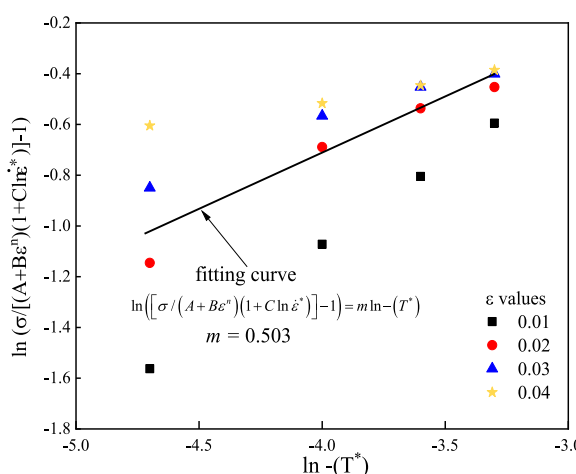


Fig. 11. The relationship between  $\ln(\sigma / [(A + B\dot{\varepsilon}^n)(1 + C \ln \dot{\varepsilon}^*)] - 1)$  and  $\ln -T^*$ .

Table 5

Original Johnson-cook constitutive model parameters of TiZrHfCu0.5 high entropy alloy.

Parameter	A (MPa)	B (MPa)	n	C	m
Value	969	1076	0.90	0.0024	0.503

at room temperature is shown in Fig. 12. As can be seen from the figure, the stresses derived from the predicted curves increase with the increase of strain rate, which is consistent with the dynamic mechanical behavior of the experimental specimens and satisfies the strain rate hardening effect. However, as the strain rate increases, the error between the simulation and experimental data increases. When the strain rate reaches  $2600\text{s}^{-1}$ , the dynamic behavior of the specimen cannot be accurately reflected.

Fig. 13 shows the experimental stress-strain curves and original Johnson-Cook model predicted curves at different temperatures. Due to the inaccuracy of the original Johnson-Cook model parameters at high strain rates, there is a significant error between the experimental results and predicted curves at low temperatures. The error may be due to the fact that the original Johnson-Cook model assumes that strain hardening, strain rate hardening and temperature are three independent units and can be isolated from each other for materials. In fact, the coupling effect between strain, strain rate and temperature should be considered.

#### 4.2. Modified Johnson-Cook model

With the increase of strain rate, there are significant differences between experimental stress-strain curves and original Johnson-Cook model predicted curves. In this section, a modified Johnson-Cook model is proposed considering the coupling effects of strain, strain rate and temperature on the material dynamic mechanical behavior.

##### 4.2.1. Term of strain hardening

In order to reflect the coupling effect of yield strength and strain hardening on the true stress during quasi-static compression, the strain hardening term is modified.

$$\sigma = A + B_1\varepsilon + B_2\varepsilon^2 \quad (13)$$

Where A is the yield strength,  $B_1$  and  $B_2$  are both strain hardening coefficients. The values of coefficients for term of strain hardening are obtained by fitting, as shown in Table 6.

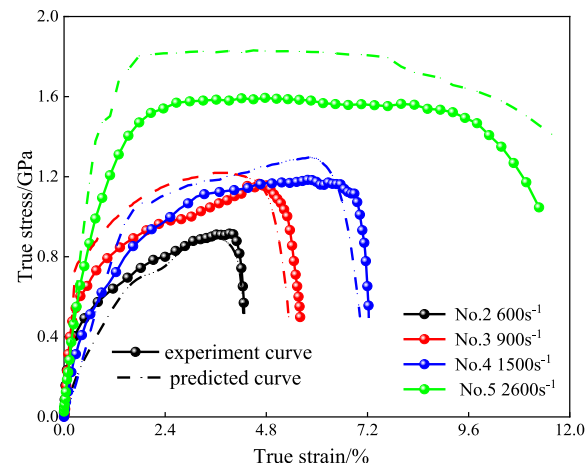
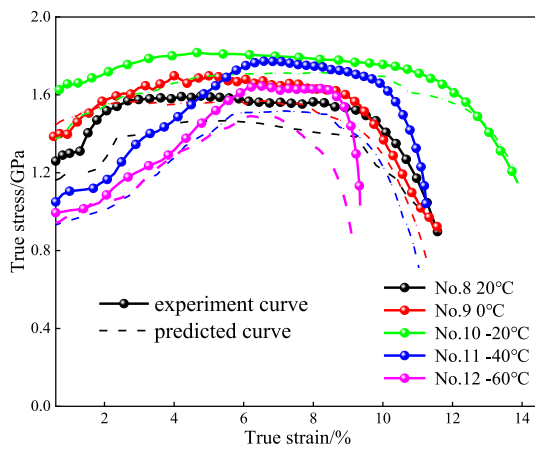


Fig. 12. Comparison between SHPB experimental results and original Johnson-Cook model predicted curves with different strain rates at room temperature.



**Fig. 13.** The experimental stress-strain curves and original Johnson-Cook model predicted curves at different temperatures.

**Table 6**  
The values of coefficients for term of strain hardening.

Coefficient	A	B <sub>1</sub>	B <sub>2</sub>
Value/MPa	898	237.02	-83.25

#### 4.2.2. Term of strain rate hardening

In the calculation of the original Johnson-Cook model, C is expressed as the average of the strain rate hardening constants at different strain rates, which makes the predicted results deviate from the experimental results. In the modified Johnson-Cook model, an equation considering the influence of strain and strain rate on the strain rate hardening coefficient is proposed, and its expression is as follows.

$$C(\varepsilon, \ln \dot{\varepsilon}^*) = C_0 + C_1 \varepsilon + C_2 \ln \dot{\varepsilon}^* + C_3 \varepsilon^2 + C_4 \varepsilon \ln \dot{\varepsilon}^* \quad (14)$$

$C_0, C_1, C_2, C_3$  and  $C_4$  can be determined by regression equation. The coefficients are calculated from the experimental data with different strain rates at room temperature as shown in **Table 7**.

#### 4.2.3. Term of thermal softening

Considering the coupling effect of strain and temperature, the temperature term is modified.

$$f(\varepsilon, T^*) = 1 - m_0(T^*)^{(m_1+m_2\varepsilon)} \quad (15)$$

Since the strain hardening and strain rate hardening terms in the modified Johnson-Cook model have been determined, the coefficients of  $m_0, m_1$  and  $m_2$  can be calculated from the experimental data, as shown in **Table 8**.

#### 4.2.4. Parameter verification of modified Johnson-cook constitutive model

The modified Johnson-Cook model considering the coupling effects of strain, strain rate and temperature can be expressed as

$$\sigma = (898 + 237.02\varepsilon - 83.25\varepsilon^2)(1 + C(\varepsilon, \ln \dot{\varepsilon}^*) \ln \dot{\varepsilon}^*) \times [1 - 2.56(T^*)^{(0.0864-1.3807\varepsilon)}] \quad (16)$$

The true stress-strain results of the modified Johnson-cook constitutive model compared with the experiment results are shown in **Fig. 14**. Considering the coupling effect of strain, strain rate and temperature,

**Table 7**  
The values of coefficients for term of strain rate hardening.

Coefficient	C <sub>0</sub>	C <sub>1</sub>	C <sub>2</sub>	C <sub>3</sub>	C <sub>4</sub>
Value	0.01318	0.27293	0.19985	0.17046	0.21515

**Table 8**

The values of coefficients for term of thermal softening.

Coefficient	m <sub>0</sub>	m <sub>1</sub>	m <sub>2</sub>
Value	2.56	0.08641	-1.3807

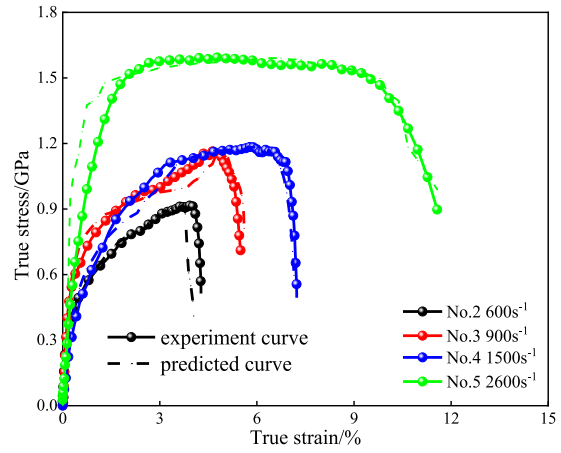


**Fig. 14.** The true stress-strain results of the modified Johnson-cook constitutive model compared with the experiment results.

the stresses obtained by experiment and modified Johnson-cook constitutive model are basically consistent at high strain rate.

**Fig. 15** shows the comparison between the modified Johnson-cook constitutive model predicted curves and experimental results at different temperatures. Considering the coupling effects of strain, strain rate and temperature, the experimental data of high strain rate at low temperatures are basically in agreement with the modified Johnson-cook constitutive model predicted curves.

#### 5. Comparison of experimental and numerical simulation results

##### 5.1. Comparison of simulation and experimental stresses at different strain rates

In order to verify the accuracy of the modified Johnson-cook constitutive model, **Fig. 16** shows the comparison between the numerical simulation and experimental results of the stress time history curve of TiZrHfCu0.5 high entropy alloy. As shown in **Fig. 16**, the error of peak

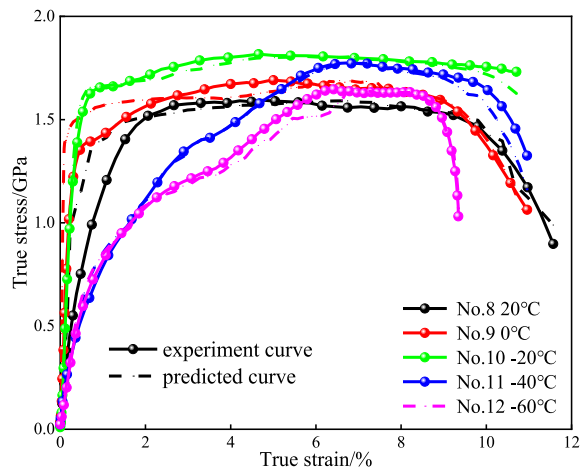


**Fig. 15.** The comparison between the modified Johnson-cook constitutive model predicted curves and experimental results at different temperatures.

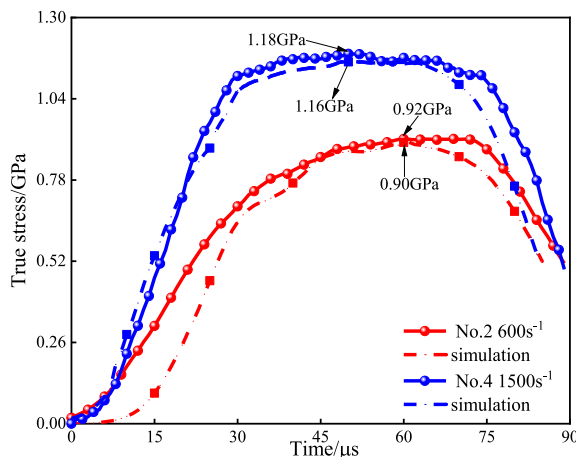


**Fig. 16.** Comparison between the numerical simulation and experimental results of the stress time history curve at different strain rates.

stress between the experimental and the simulation results at a strain rate of  $600\text{s}^{-1}$  is 2.17%; When the strain rate is  $1500\text{s}^{-1}$ , the peak stress of experimental result is 1.18 GPa, and the peak stress of simulation result is 1.16 GPa, with an error of 1.69 %. It shows that the numerical simulation results of the modified Johnson-cook constitutive model are reliable.

Figs. 17 and 18 show the simulation results of stress nephogram at strain rates of  $600\text{s}^{-1}$  and  $1500\text{s}^{-1}$ , respectively. According to Fig. 17, six different moments during the action time of the first stress wave are extracted. From Fig. 17, it can be seen that the stress wave passes through the specimen at  $t = 15\mu\text{s}$ . As the duration of stress wave action continues, the stress continues to increase. At  $t = 60\mu\text{s}$ , the stress reaches a maximum value of 0.9 GPa. At  $t = 70\mu\text{s}$ , the stress begins to decrease, and the specimen reaches the unloading stage, which is consistent with the experiment. From Fig. 18, it can be seen that the first stress wave is approaching the end of the specimen at  $10\mu\text{s}$ . At  $t = 50\mu\text{s}$ , the stress reaches a maximum value of 1.16 GPa. Subsequently, the stress continues to decrease. In addition, from the stress nephogram at different strain rates, it can be seen that the specimen has a significant strain rate hardening effect with the increase of strain rate.

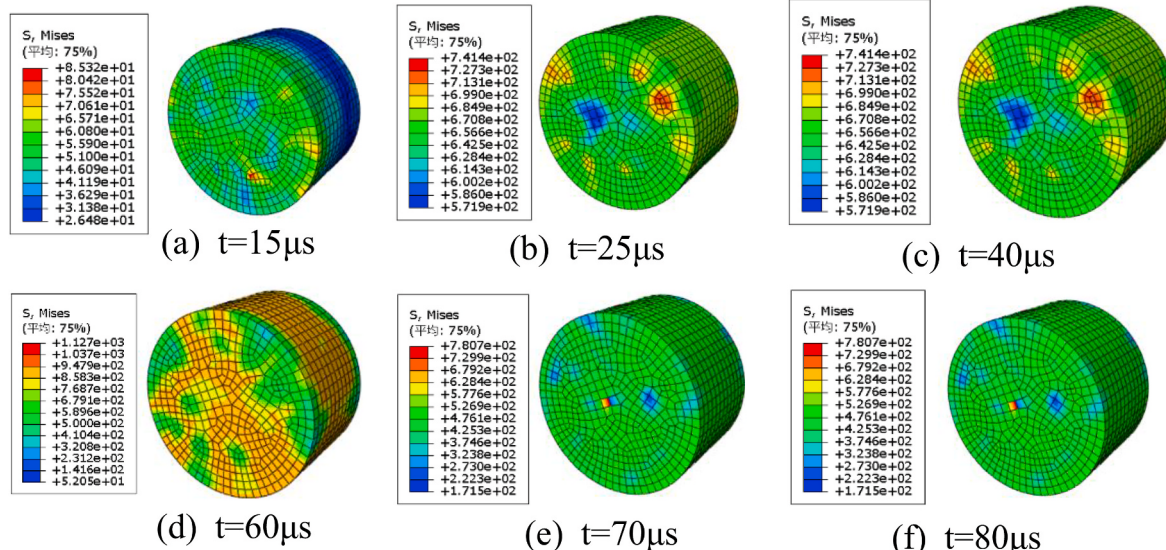


**Fig. 17.** Stress nephogram at strain rate of  $600\text{s}^{-1}$ .

## 5.2. Comparison of simulation and experimental stresses at different temperatures

In order to verify the accuracy of the modified Johnson-cook constitutive model under low temperature conditions, the stress-strain curves of the specimens at different temperatures ( $0^\circ\text{C}$  and  $-40^\circ\text{C}$ ) with the same strain rate are compared, as shown in Fig. 19. The results show that the stress-strain curves of simulation and experiment are in good agreement. The modified Johnson-cook constitutive model considering the coupling effect of strain, strain rate and temperature can accurately predict the dynamic mechanical behavior of high entropy alloy.

Fig. 20 shows the comparison between the numerical simulation and experimental results of No. 10 specimen. The compressed images of No.10 specimen collected by high-speed camera at different moments are compared with the simulation results, as shown in Fig. 21. At the initial moment, the specimen is not affected by the stress wave in the static state, and the stress is 0; when the first stress wave is introduced into the specimen from the incident bar, the stress and strain of the specimen begin to increase. At  $t = 5\mu\text{s}$ , the stress of the specimen in the elastic stage is 50 MPa, which is almost consistent with the experiment. With the increase of stress, the yield stage is reached at b point, and the stress is 1.49 GPa; due to the influence of strain hardening effect, with the increase of time, the specimen reaches the strengthening stage. The peak stress of numerical simulation at  $t = 45\mu\text{s}$  is 1.79 GPa, and the error is 1.6 % compared with the experimental peak stress. In the unloading stage, the stress of the specimen begins to decrease with the increase of time, which is consistent with the experimental results.

## 5.3. Relative error analysis

In order to further verify the reliability and accuracy of the numerical simulation of the modified Johnson-Cook model, the amount average relative error (AARE) is calculated. The expression is as follows.

$$AARE(\%) = \frac{1}{N} \sum_{i=1}^N \left| \frac{E_i - P_i}{E_i} \right| \times 100 \quad (17)$$

Where  $P_i$  is the predicted value of the model, and  $E_i$  is the corresponding experimental data.  $N$  is the total amount of data. Table 9 shows AARE of original Johnson-Cook model (OJCM) and modified Johnson-Cook model (MJCM) for different strain rates at room temperature. Table 10 shows AARE of original Johnson-Cook model (OJCM) and

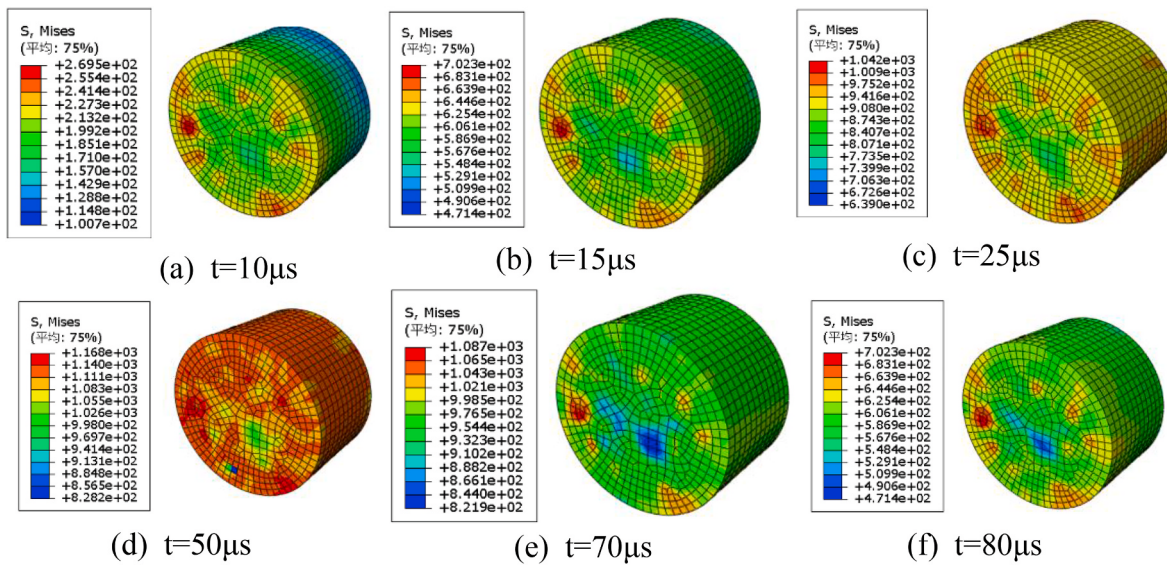
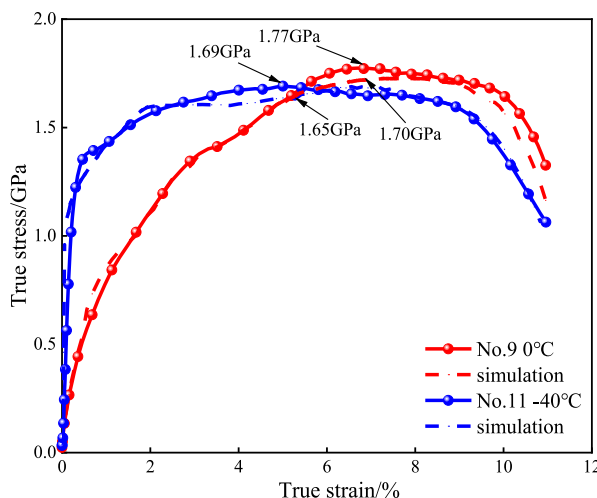
Fig. 18. Stress nephogram at strain rate of  $1500\text{ s}^{-1}$ .

Fig. 19. Comparison between the numerical simulation and experimental results of the stress-strain curves at different temperatures.

modified Johnson-Cook model for different temperatures at strain rate  $2600\text{ s}^{-1}$ .

The results show that the error between the predicted values of the modified Johnson Cook constitutive model and the experimental data is significantly smaller than that of the original Johnson-Cook constitutive model. According to Figs. 16 and 19, the modified Johnson-Cook constitutive model can accurately reflect the true stress of TiZrHfCu0.5 high entropy alloy at high strain rates and low temperatures.

## 6. Conclusions

In summary, the compression properties of TiZrHfCu0.5 high entropy alloy at different strain rates and temperatures were tested by universal testing machine and SHPB experimental system. Based on the experimental results, the parameters of the original Johnson-Cook and modified Johnson-Cook constitutive models were determined. The modified Johnson-Cook constitutive model parameters were applied to ABAQUS finite element software, and the dynamic compressive mechanical behavior of high entropy alloy was numerically simulated. The accuracy of the modified Johnson-Cook constitutive model was verified by comparing the simulation results with the experimental results. The following conclusions were drawn.

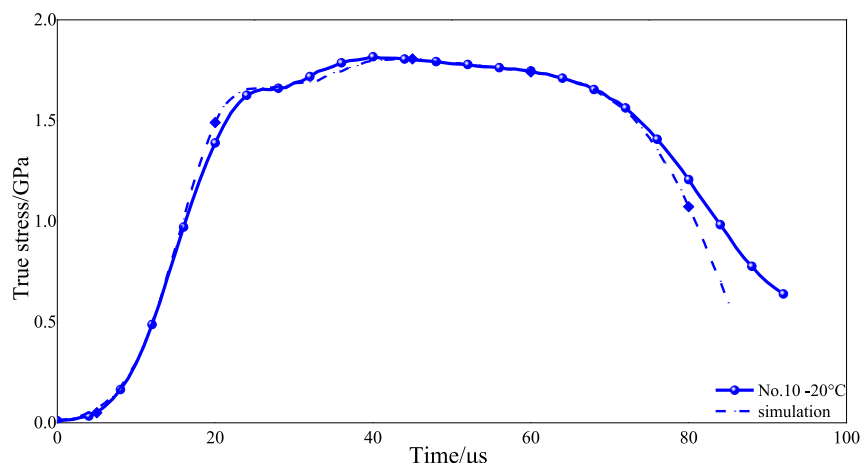
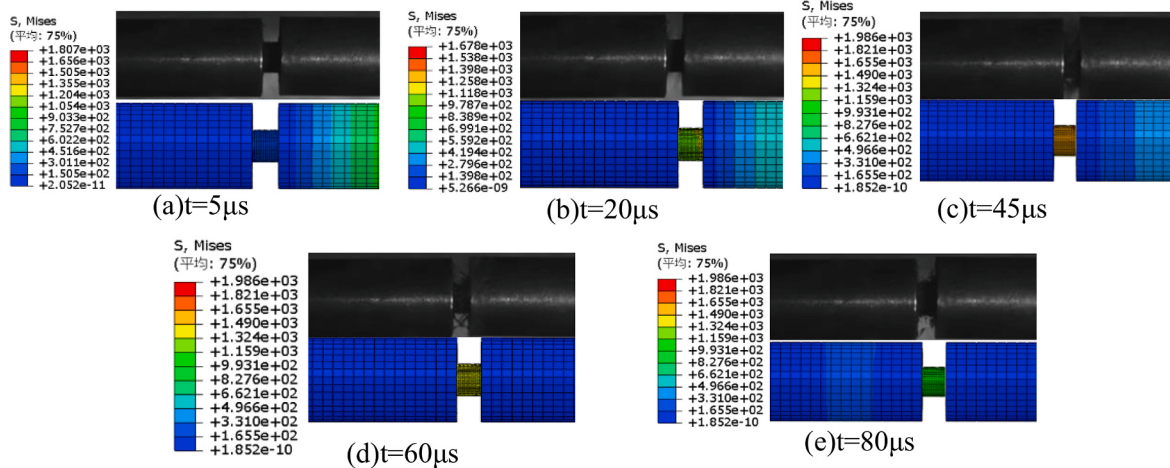


Fig. 20. Comparison between the numerical simulation and experimental results of No. 10 specimen.



**Fig. 21.** The comparison of specimen morphology obtained by No. 10 experiment and numerical simulation at different moment.

**Table 9**

AARE of original Johnson-Cook model (OJCM) and modified Johnson-Cook model (MJCM) for different strain rates at room temperature.

Strain rate/s <sup>-1</sup>	600	900	1500	2600
OJCM_AARE (%)	1.80	4.09	9.59	14.94
MJCM_AARE (%)	1.69	2.17	1.96	0.28

**Table 10**

AARE of original Johnson-Cook model (OJCM) and modified Johnson-Cook model for different temperatures at strain rate 2600 s<sup>-1</sup>.

Temperature/°C	0	-20	-40	-60
OJCM_AARE (%)	7.84	5.18	14.39	9.67
MJCM_AARE (%)	0.15	0.65	0.18	0.48

- (1) During dynamic loading, TiZrHfCu0.5 high entropy alloy exhibited a significant strain rate hardening effect. The yield stress could reach 1.32 GPa under the strain rate of 2600 s<sup>-1</sup>. Due to the existence of chemical short-range order during dynamic loading, TiZrHfCu0.5 exhibited excellent mechanical properties at low temperatures. The ultimate stress of the specimen could reach 1.79 GPa at -20 °C.
- (2) The parameters A, B, n, C, and m of the original Johnson-Cook constitutive model were determined by fitting the stress-strain curve. On this basis, considering the coupling effects of strain, strain rate and temperature on the dynamic mechanical behavior of materials, a modified Johnson-Cook constitutive model was proposed and the corresponding parameters were determined. The experimental data of high strain rate at low temperature were basically consistent with the predicted curves of the modified Johnson-cook constitutive model.
- (3) Based on the modified Johnson-Cook constitutive model, the dynamic compression process of high entropy alloy under corresponding experimental conditions was numerically simulated by ABAQUS finite element software. The comparison between numerical simulation and experimental results showed that the modified Johnson-Cook constitutive model could better predict the compression performance of TiZrHfCu0.5 high entropy alloy at high strain rate and low temperature. Compared with the original Johnson-Cook constitutive model, the relative error of the predicted results of the modified Johnson-Cook constitutive model was greatly reduced.

## Data availability

The data that support the findings of this study are available from the corresponding author upon reasonable request.

## Declaration of competing interest

The authors declare that they have no known competing financial interests or personal relationships that could have appeared to influence the work reported in this paper.

## Acknowledgements

The research was supported by National Natural Science Foundation of China (12102272). Thanks to Key Laboratory of Transient Physical Mechanics and Energy Conversion Materials of Liaoning Province for their support during the experiments, especially for the efforts of graduate students in experimental measurements.

## References

- [1] Miracle DB, Senkov ON. A critical review of high entropy alloys and related concepts. *Acta Mater* 2017;122:448–511.
- [2] Zhang Y, Zuo TT, Tang Z, et al. Microstructures and properties of high-entropy alloys. *Prog Mater Sci* 2014;61:1–93.
- [3] Gao MC, Carney CS, Dogan Ö N, Jablonksi PD, Hawk JA, Alman DE. Design of refractory high-entropy alloys. *J Occup Med* 2015;67(11):2653–69.
- [4] Lilienstein L, Couzinie JP, Perrière L, et al. New structure in refractory high-entropy alloys. *Mater Lett* 2014;132:123–5.
- [5] Hu ML, Song WD, Duan DB, Wu Y. Dynamic behavior and microstructure characterization of TaNbHfZrTi high-entropy alloy at a wide range of strain rates and temperatures. *Int J Mech Sci* 2020;182:105738.
- [6] Wang SB, Wu MX, Shu D, et al. Mechanical instability and tensile properties of TiZrHfNbTa high entropy alloy at cryogenic temperatures. *Acta Mater* 2020;201:517–27.
- [7] Chen JL, Chen C, Guo K, et al. Dynamic mechanical properties and ignition behavior of TiZrHfX0.5 high-entropy alloys associated with temperature, trace element and strain rate. *J Alloys Compd* 2023;933:167798.
- [8] Ren KR, Liu HY, Ma R, et al. Dynamic compression behavior of TiZrNbV refractory high-entropy alloys upon ultrahigh strain rate loading. *J Mater Sci Technol* 2023;161:201–19.
- [9] Sun J, Zhao WX, Yan P, et al. Effect of temperature and strain rate on quasi-static and dynamic compressive behavior of forged CrMnFeCoNi high entropy alloy. *Mater Sci Eng, A* 2023;870:144846.
- [10] Zhong XZ, Zhang QM, Ma MZ, et al. Dynamic compressive properties and microstructural evolution of Al1.19Co2CrFeNi1.81 eutectic high entropy alloy at room and cryogenic temperatures. *Mater Des* 2022;219:110724.
- [11] Yuan KB, Yao XH, Yu YQ, Wang RF, Chai ZS, Zhou KX, et al. Dynamic thermomechanical response and constitutive modeling of eutectic high-entropy alloy. *Int J Mech Sci* 2023;246:108148.
- [12] Zhao D, Fang HQ, Jin T, Zhang TW, Chen G, Ma SG, et al. Constitutive modeling and strain hardening of CoCrFeNiAlx high-entropy alloys. *Mater Res Express* 2019;6:1065h3.

- [13] Wang YY, Wang JD, Lei MQ, et al. A crystal plasticity coupled damage constitutive model of high entropy alloys at high temperature. *Acta Mech Sin* 2022;38:122116.
- [14] Brown C, McCarthy T, Chadha K, et al. Constitutive modeling of the hot deformation behavior of CoCrFeMnNi high-entropy alloy. *Mater Sci Eng, A* 2021;826:141940.
- [15] Zhang TW, Jiao ZM, Wang ZH, Qiao JW. Dynamic deformation behaviors and constitutive relations of an AlCoCr1.5Fe1.5NiTi0.5 high-entropy alloy. *Scripta Mater* 2017;136:15–9.
- [16] Kim Y, Park HK, Asghari-Rad P, et al. Constitutive modeling with critical twinning stress in CoCrFeMnNi high entropy alloy at cryogenic temperature and room temperature[J]. *Met Mater Int* 2021;27:2300–9.
- [17] Wang YZ, Jiao ZM, Bian GB, et al. Dynamic tension and constitutive model in Fe40Mn20Cr20Ni20 high-entropy alloys with a heterogeneous structure[J]. *Mater Sci Eng, A* 2022;839:142837.
- [18] Sun ZR, Shi CG, Xiao XK, et al. Investigation of mechanical behavior, constitutive modeling, and fracture criteria for as-cast Al0.3CoCrFeNi high entropy alloy. *Intermetallics* 2023;162:108029.
- [19] Jain R, Umre P, Sabat RK, et al. Constitutive and artificial neural network modeling to predict hot deformation behavior of CoFeMnNiTi eutectic high-entropy alloy. *J Mater Eng Perform* 2022;31(10):8124–35.
- [20] Huang AM, Fensin SJ, Meyers MA. Strain-rate effects and dynamic behavior of high entropy alloys. *J Mater Res Technol* 2023;22:307–47.
- [21] Meyers MA. Dynamic behavior of materials[M]. John Wiley & Sons; 1994.
- [22] John GR, Cook WH. Fracture characteristics of three metals subjected to various strains, strain rates, temperatures and pressures. *Eng Fract Mech* 1985;21(1):31–48.
- [23] Taylor G. Thermally-activated deformation of BCC metals and alloys. *Prog Mater Sci* 1992;36:29–61.
- [24] Singh P, Smirnov AV, Johnson DD. Atomic short-range order and incipient long-range order in high-entropy alloys. *Phys Rev B* 2015;91:224204.
- [25] Ding QQ, Zhang Y, Chen X, Fu XQ, Chen DK, Chen S.J., et al. Tuning element distribution, structure and properties by composition in high-entropy alloys. *Nature* 2019;574(7777):223–7.